PERIODICA POLYTECHNICA SER. MECH. ENG. VOL. 37, NO. 1, PP. 3-27 (1993)

CHARACTERIZATION OF STRUCTURE AND CORROSION BEHAVIOR OF ELECTRON BEAM TREATED STAINLESS STEELS

HAMID S. MAHDI

Technical University of Budapest
Department of Mechanical Technology and Materials Science
H-1521 Budapest, Hungary

Received: December 22, 1992

Abstract

Specimens of (AISI 321Ti and 420) stainless steels treated by high energy Electron Beam (EB) have been examined to investigate the change in microstructure, and its influence on the mechanical properties, and corrosion behavior in two different environments. The EB treatments have been performed with different working conditions, (incident power density, traverse speed, pattern-shaped deflections, etc.) that affected the obtained microstructure.

The EB treated layers have shown almost completely novel, refined structure, comparing with the base material, and — as a result — the surface properties have been changed. The hardness curves of (AISI 321Ti), haven't shown considerable differences between the EB treated layers and the base material. In the case of (AISI 420), more than usual increase of hardness in treated surface layers could be observed.

Keywords: stainless steels, electron beam local treating, rapid cooling, microstructure, surface properties.

Introduction

The High Energy Sources (HES), such as laser beam, electron beam, plasma techniques, offer good operability of precision control of heat input, and its high density, in wide range. The HES surface treatment [1] is one of the important applications of the HES material processing [2].

Although many researchers have investigated the characteristics of HES surface treating of steels [3–7], and stainless steels, too [8–10], relatively less work has been focused on detailed microstructural changes after EB treating, and less studies include the effects of EB on the corrosion resistance of the treated surface layers, especially of the stainless steels, thus the austenitic (AISI 321Ti), and martensitic (AISI 420) stainless steels were employed in this investigation.

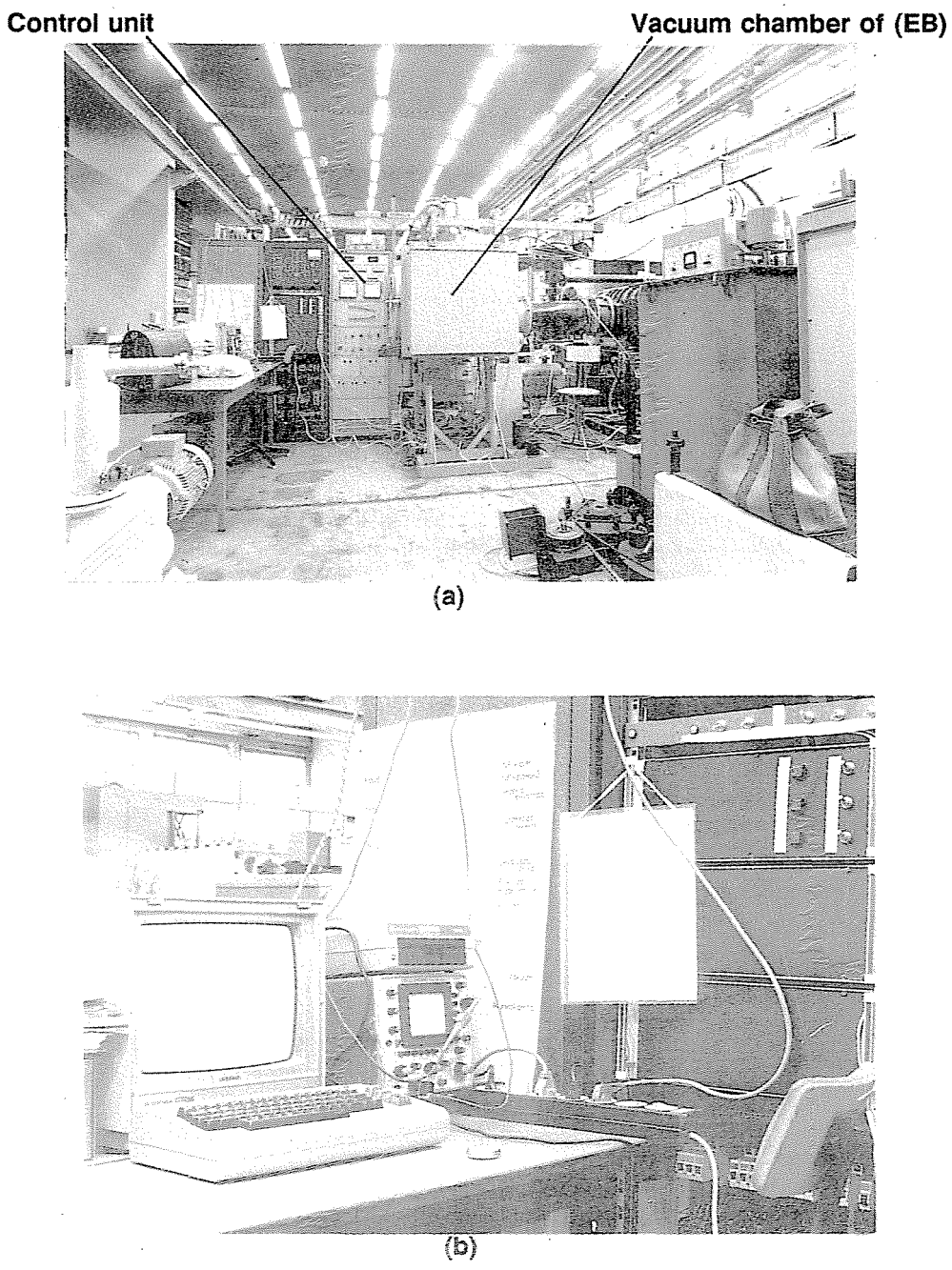

Fig. 1. Electron Beam (EB) unity, type: (ES-H60/60-Mo7)
a) Complete unity of employed (EB)
b) Programming the (EB) deflection

Experimental Procedures

The chemical composition of the examined stainless is shown in *Table 1*. All the specimens used in our experiments were prepared as follows:

- AISI 321Ti specimens were prepared as thick plates, each of them has a thickness of 13 mm, width of 100 mm and a length of 100 mm.
- AISI 420 specimens were obtained from a rotational bar of 42 mm diameter, and length of 30 mm, for each specimen.

Table 1
The chemical composition (wt %) of AISI types 321Ti & 420

Stainless steel type	Chemical Composition (wt %)									
	C	Cr	Mn	Mo	Nb	Ni	P	S	Si	Ti
AISI 321Ti	0.09	18.1	1.36	0.08	0.05	10.7	0.033	0.016	0.35	0.69
AISI 420	0.25	12.65	0.55	0.04	*	0.26	0.01	0.02	0.42	*

* Others: Co, Cu, V, W, Nb, Ti

The treatments were performed by high energy EB equipment type: (ES–H 60/60–Mo7) where:

$$U_{\max} = 60 \text{ kV},$$
$$I_{\max} = 125 \text{ mA}.$$

The electron gun heating takes place in a vacuum chamber (*Fig. 1a*), and vacuum locks permitting admission and draw all of individual required components. The electron gun allows programmed beam deflection by programming unit (*Fig. 1b*) in two directions, as zigzag line-shaped, continuous circular-shaped, united center circle-shaped and multi-points-shaped patterns, with different parameters of technologies (*Table 2* and *Table 3*).

However, before the electron beam treating all the specimens were firstly preheated to 250°C to avoid high thermal gradients and high stresses during rapid heating that may cause warpage and cracking in these thickness sections. *Figure 2* shows the surface tracks of EB local melted layers of austenitic specimens, while the EB tracks on martensitic specimens are demonstrated in *Fig. 3*.

After the surface treatment processes, a slow cutting rate with water cooling was utilized to minimize deformation induced during cutting of all the specimens in order to examine and evaluate the effectiveness of EB on surface properties of the selected materials. Cross-sectional samples were prepared for hardness, microhardness measurements, optical microscopy (OM), scanning electron microscopy (SEM), and X-ray spectrum examination for metal control (chemical composition analysis).

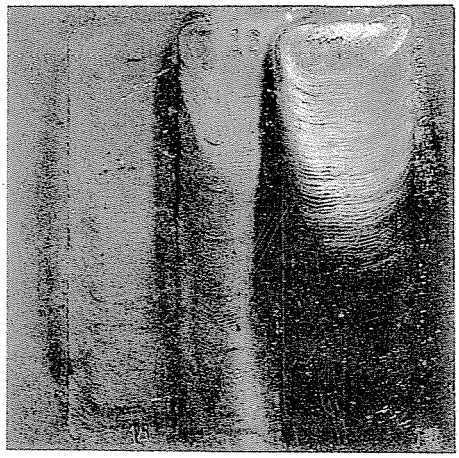

Technology No. 1E & 2E

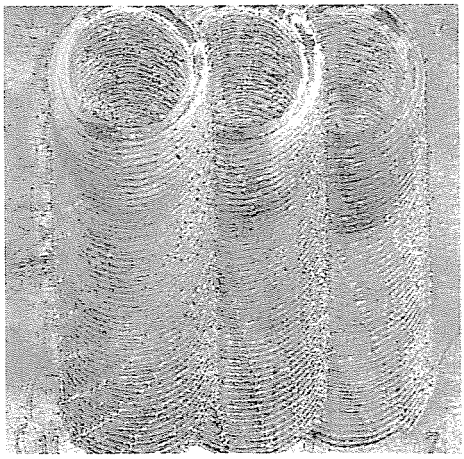

Technology No. 3E & 4E

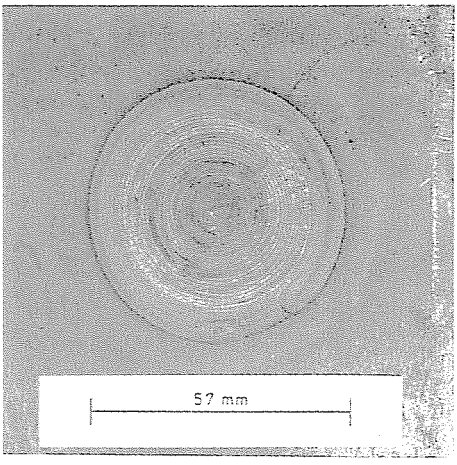

Technology No. 5E & 6E

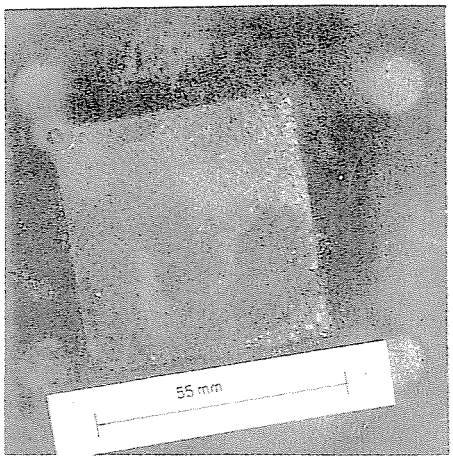

Technology No. 7E & 8E

Fig. 2. Surface tracks of electron beam local melted layers for austenitic stainless steels (AISI 321Ti).

Technology No. 1E

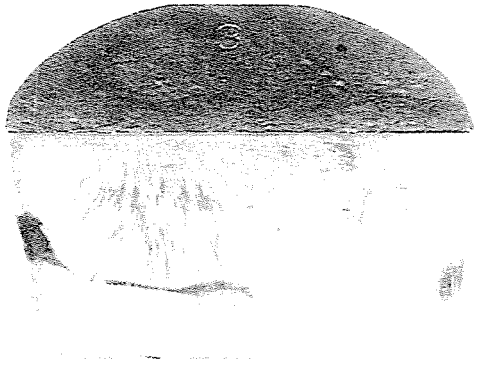

Technology No. 2E

Fig. 3. Surface tracks of electron beam local treating layers for martensitic stainless steels (AISI 420).

The treated surface layers were optically analyzed and mechanically tested, then exposed to local corrosive testing, to study their corrosion resistance after the treatment processes, and consequently to compare the effects with each other, as well as the different technologies to define the better one for the required properties.

In addition to the conventional optical microscopy, scanning electron microscopy techniques were extensively used to study the changing in the microstructure of new surface layers, while the scanning electron

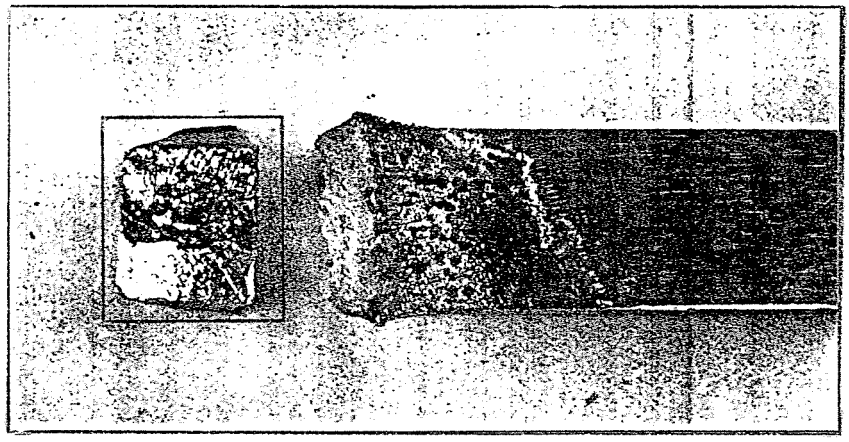

(a)

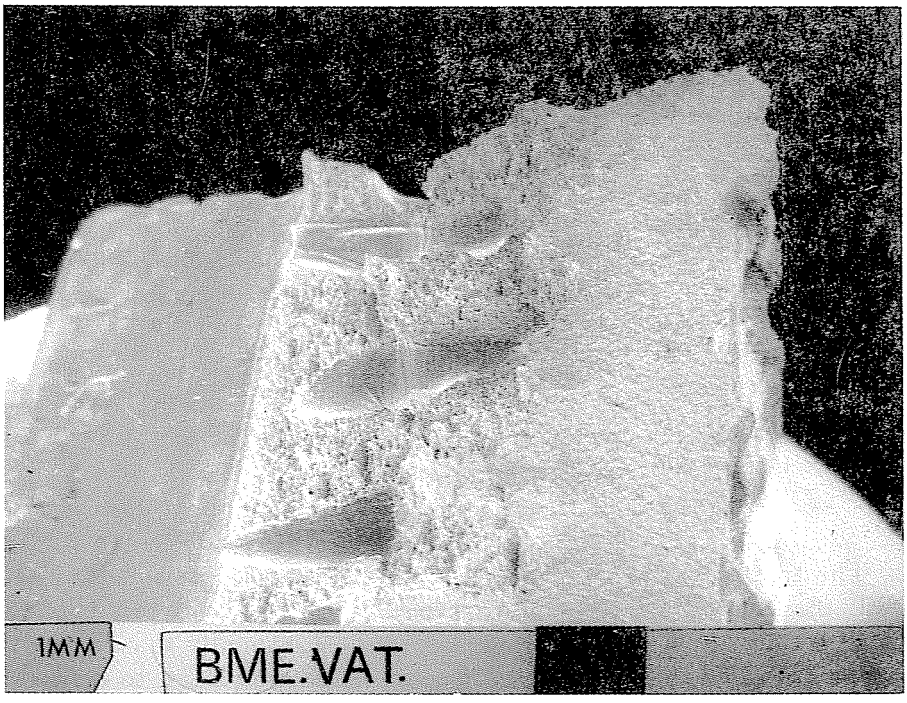

(b)

Fig. 4. Broken Charpy specimen, has tracks of localized corrosion treating
a) Small sample obtained from the Charpy specimen
b) Fracture surface of (SEM) sample.

microscopy offers possibilities for image formation that are usually easy to interpret and will reveal clear pictures of as-polished and etched cross-section, as well as rough surfaces.

Small samples having 6 to 8 mm length of cross-section 8×8 mm were obtained from the non-standard of the broken (Charpy) specimens which were mainly cut from the treated side of the specimens to involve the affected surface layers (*Fig. 4a*). This small piece (*Fig. 4b*) was fixed on a special small disc to introduce them into a vacuum chamber of the SEM where the disc can be rotationally moved to see more than one side of the tested piece. The microstructure was analyzed by a 'JEOL–JSM–35' type scanning electron microscope ($U = 15$ kV, $I = 2 - 20$ mA).

Metal Control: The purpose of these examinations was to study the effect of rapid surface heating by high energy sources, and the cooling rate during the solidification on distribution of the different phases and the alloying elements in the treated surface layers of the selected specimens. As the temperature and cooling rate change with the treated surface, the specimens were polished prior to every examination, SiC polishing papers to grade 800 μm and aluminia powder to grade 0.05 μm were the polishing materials, for etching Nital 5% was used.

'AMRAY 1830 I DIGITAL IMAGING COMPUTER CONTROLLED' type SEM was employed for this purpose. The diffractometer was controlled by a computer via an 'AMRAY 1830 I' processor. The automatic contrast and brightness system quickly adjusts the video signal levels to variation occurring normally by changing the lens setting, kV, gun bias aperture, size sample tilt, and detector voltages. Incorporating 512×512 ×16 bit image storage, with Frame Buffer of process images from any of number of standard and optional detector is available with AMRAY 1830. These include the secondary Electron detector (with variable collector bias for backscattered electron imaging), Solid State BSE Quad detector, Cathodo-luminescence detector, X-ray detectors, etc.

Our specimens were prepared to optical microscopy in order to measure their hardness levels by microhardness measurement methods when the conventional (Vickers) hardness measuring method is insufficient to evaluate the change in hardness levels, depending on thickness of treated surface layers, and the required accuracy of the distributed hardness measurements across this thickness. The corrosion behavior of treated and untreated corroded surfaces were observed by the scanning electron microscope.

Two different laboratory corrosion testing methods were employed in this experimental work to evaluate the effects of high energy sources surface treatments on the corrosion resistance of austenitic (AISI 321Ti) stainless steels, these corrosive testing methods are as follows.

Localized Corrosion Testing (Pitting Testing)

This method was carried out for all the specimens of (Ti stabilized austenitic) stainless steels which were already treated by EB. Using the pickling bath for 30 minutes, the surfaces of these specimens were cleaned; the pickling bath contains:

1000 cm^3	H_2O,
210 cm^3	HCl, ($\rho = 1.19\,g/cm^3$)
10 g	$(CH_2)_6H_4$
5 g	CH_4N_2S

Then the specimens were exposed to localized corrosion testing by the acidic solution of (nitrohydrochloric acid) for reaction time of 14 days. *Figure 5* schematically shows the localized corrosive experiment, the acidic solution (corrosive medium), contains:

30 ml	HCl	1:19
15 ml	HNO_3	37%
3 ml	$C_3H_8O_3$	87%

The purpose of this testing is to evaluate the pitting corrosion behavior of the treated surface layers because the pitting is considered as a form of localized corrosion. All the testing processes were performed at room temperature. The corroded surfaces are usually photographed, the size, and the density of the pits are determined according to *Fig. 6* [11].

Accelerated corrosion tests were often conducted at temperatures above the proposed operating temperatures in order to decrease the time of testing; this procedure is dangerous because the effect of temperature may be great, resulting in the elimination of more economical material.

Intergranular Corrosion Testing

Susceptibility to intergranular attack depends on the corrosive solution and on the extent of intergranular precipitation, which is a function of alloy composition, fabrication, and heat treatment parameters. Corrosion tests for evaluating the susceptibility of an alloy to intergranular attack are typically classified as either simulated service or accelerated test. The first laboratory tests for detecting intergranular attack were simulated service exposures. These were first observed and used in 1926 when intergranular attack was detected in an austenitic stainless steel in copper sulfate-sulfuric acid ($CuSO_4$–H_2SO_4) pickling tank [12].

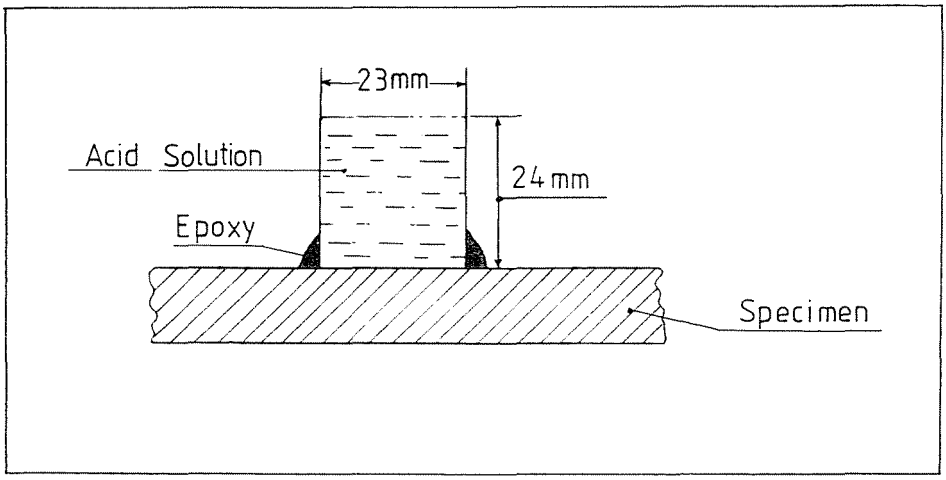

Fig. 5. Schema of localized corrosion testing of Nitro-Hydrochloric corrosive media for period of 14 days

Another simulated service test for alloys intended for service in nitric acid (HNO_3) plants is described [13]. In this case, for accelerated results, Iron-Cr alloys were tested in a boiling 65% HNO_3 acidic solution. In this corrosion testing, two samples of 5 mm thick strip, 20 mm wide, and 85 mm long were cut from two differently treated austenitic specimens having two different EB tracks of technologies (1E & 3E). These prepared samples were ground on emery paper after cutting them from the original specimens and grinding the treated surface faces, then they were subjected to boiling for 24 hours in acidic solution of:

160 ml ($CuSO_4 \times 5H_2O$)
100 ml (H_2SO_4), ($\rho = 1.84\,g/cm^3$)
1000 ml (H_2O)
50 g Chip of copper

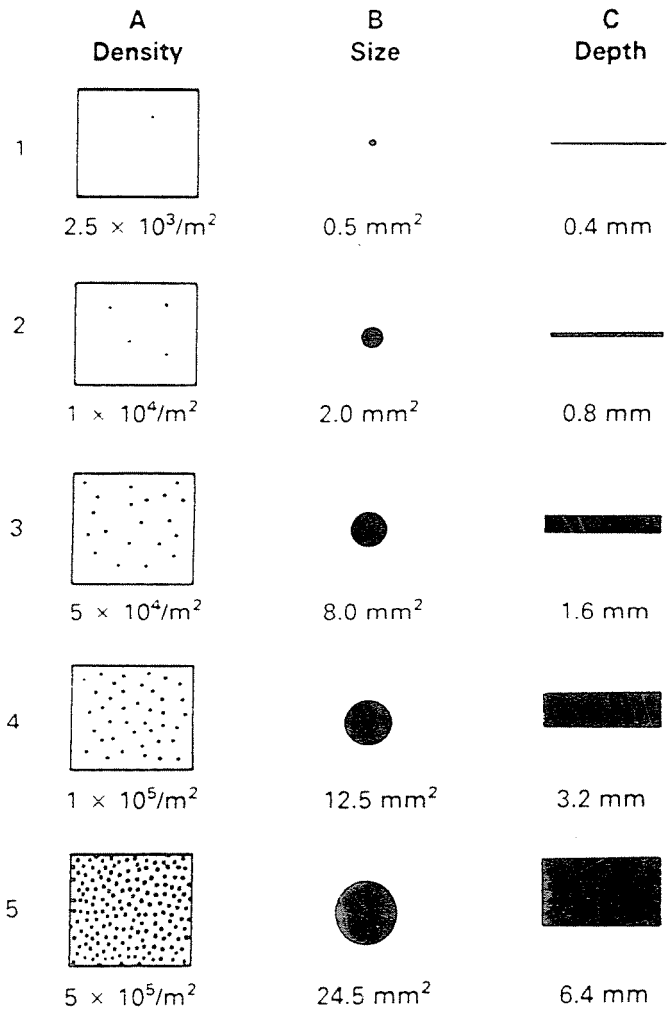

Fig. 6. Standard rating chart for pits

Experimental Results and Discussion

Effect of EB Melting on the Microstructure of Austenitic (AISI 321Ti) Specimens:

As already mentioned, the microstructure of the surface layers of austenitic specimens melted by EB processing were examined by both of light and electron optical levels. The microstructure of EB melted layers, (*Fig. 7a*) appeared to be quite different comparing with the microstructure of the base material, (*Fig. 7b*), where the difference in the grain sizes is clearly noticed. The obtained microstructure from EB surface melting layers of all the austenitic specimens was dendrite-shaped, (*Fig. 8*), however, it is strongly influenced by the cooling rates at solidification that vary with the difference of the EB parameters, and consequently with the depth of the melted layers.

Therefore the dendrite coarseness has a strong dependence on cooling rates, and slightly on the chemical composition of the melted material. Since the chemical composition is the same for all the austenitic specimens, the main factor affecting the refinement of microstructure attributes to the depth of melted layers, and consequently to the rates of solidification during different EB technologies. The difference of microstructure across these melted layers was determined primarily by the depth of EB melted layers, (see *Table 2*), then by measurement of dendrite arm spacing for two of different dendritic microstructure shapes which were already created using two EB technologies (7E & 5E).

Table 2
Parameters and shapes of EB surface treatments for austenitic specimens

No. of techn.	Focus current I_f [A]	Beam current I_b [mA]	Acceleration voltage U [kV]	Workpiece speed V [mm/min]	EB Frequ. /t f/s	EB deflection	Depth of melted layer [mm]
1E 2E	0.768	72	60	78	1.74 1.60		5–7
3E 4E	0.768	72	60	78	0.80 0.87		3–5
5E 6E	0.768	75 50	60	—	—		3 - 5
7E 8E	0.768	38 38	60	1 period, t = 180 s 2 period, t = 360 s			0.75–1.25

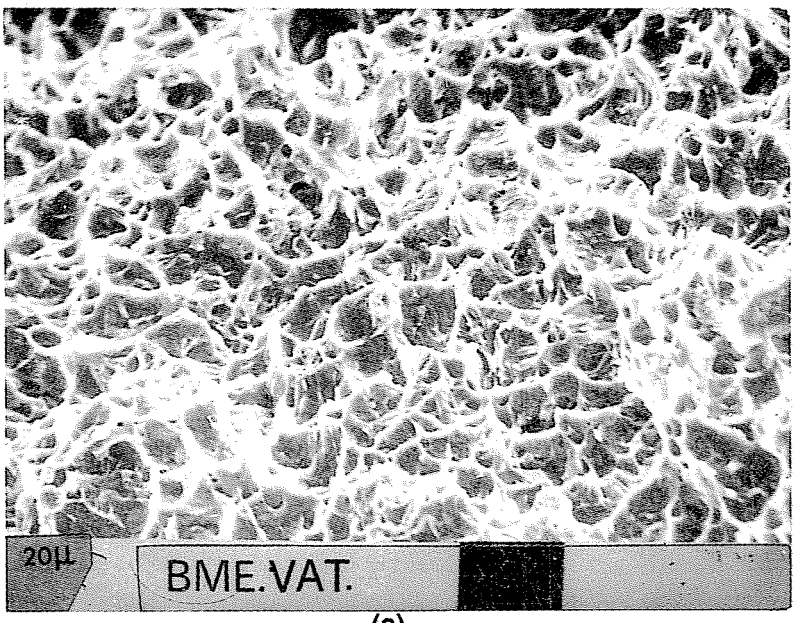

(a)

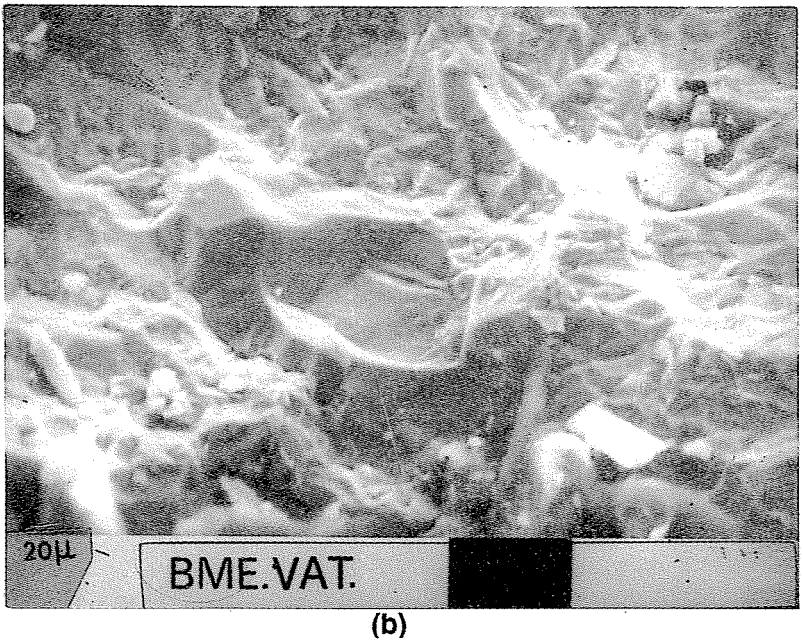

(b)

Fig. 7. (SEM) Micrographs of the Charpy fracture surface of austenitic s. s.
a) EB treated surface by Tech. (3E, 4E)
b) The base material

However, the optical analysis and the dendrite arm spacing measurements were carried out at the same depth position from the melted surface layers (0.5 mm) of these cases. While the depth of the melted layer by technology 7E: (0.75–1.25 mm), and by technology 5E: (3–5 mm), the dendrite arm spacing of the first one: ($\delta = 3\,\mu$m), and for the other technology: ($\delta = 9.60\,\mu$m), see *Fig. 9.*

Effect of EB on Hardness of Austenitic (AISI 321Ti) Specimens:

In order to examine the effect of the melting processes by EB for the surface layers of austenitic specimens on their hardness, the Vickers hardness measurements with a weight of 1 kg were made on the cross-section. The hardness profiles for all the melted layers by various parameters of EB as well as the base material of these specimens are represented in *Fig. 10.*

After each of EB melting technology of the austenitic specimens, the difference in the measured hardness is found in the range of (30–40 HV), comparing with the base material hardness. This little difference can be attributed to the changes of the microstructure into a new (refined) dendrite microstructure. These hardness profiles do not include the measurements of the $Cr_{23}C_6$, and the M_6C particles (most commonly observed from 500–950°) themselves the hardness of which is much higher (approx. 950 to 1800 HV).

In both instances dendrites identified as carbides dendrites are discernible. These were formed as a result of the partial melting of the carbides particles during their passage through the EB. Drops of the melted (carbides) entered the melted steel bath and re-solidification. Since the solidus temperature of the carbides particles is higher than the temperature of evaporation of iron (3200° compared with 2000°), these drops obviously solidified rapidly to dendrites.

Effect of EB Melting on the Toughness of Austenitic (AISI 321Ti) Specimens:

Corresponding to the change in the modes of the solidification the morphologies of microstructure changeed, whereas the refinement was obtained as a result of the EB technologies melting. According to this creation of new microstructure, the toughness of the treated surface layers is obviously improved comparing with toughness of the base material, which was tested by Charpy non-standard fracture faces for austenitic (AISI 321Ti) specimens.

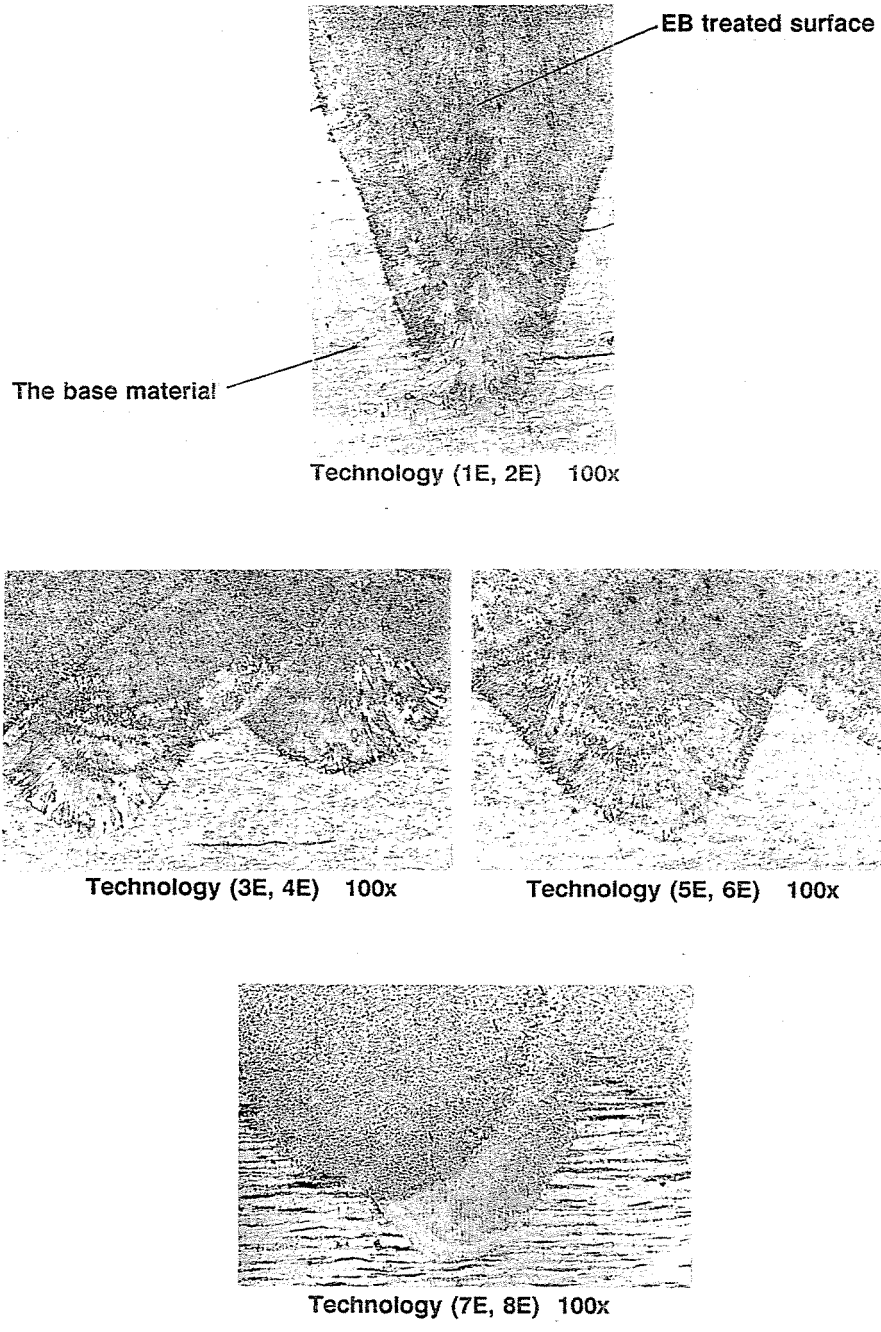

Fig. 8. (OM) Mikrographs of EB melted layers for austenitic (AISI 321 Ti) specimens.

Figure 11 shows the difference between the fracture of the base material in (a) and (b), where the brittle fracture zones clearly appear with big grains comparing with the EB refined microstructure, in (c) and (d), melted by technologies, (3E) and (7E), respectively.

Effect of EB Melting on the Corrosion Behavior of Austenitic (AISI 321Ti) Specimens:

Figure 12 shows the different localized corroded surfaces of four austenitic tested specimens. While surfaces of the specimens (No. 1, 2 and 3) were affected by EB technologies (3E, 1E and 7E), respectively, the specimen (No 4) represents the base material after the localized corrosion testing. Although the smoothness of the treated surfaces of specimens (1 and 4) is better than that of specimens (2 and 3), the resistance to pitting corrosion of the specimens (No. 1 and 4) is less than that of specimens (No. 2 and 3). More clear representation for the effectiveness of this localized (pitting) corrosion testing of three different austenitic specimens see in *Fig. 11 b, c* and *d,* however the pits in (*b*) case are wider and deeper than in the other cases. The comparison between the corrosion resistance of the base material and any treated surface by EB such as the treated surface by technology (5E) which corroded in the same conditions, is shown in *Fig. 13.*

The width and depth of the melted zones vary with the EB parameters, (beam diameter, power, the traverse speed, the deflection shape, etc.), that mainly affect refinement, smoothness of the treated surface layers and, consequently, the localized corrosion resistance. Thus the EB technology (7E, 8E) — the random multi-points EB technology — is the best one to give more refinement for the microstructure in the surface layer, more smoothness, as well as higher resistance to the pitting corrosion.

For the intergranular corrosion behavior of the tested specimen after EB melted layers by technologies (1E & 3E), (see *Fig. 14a, b*), however, this testing did not significantly affect the treated zones, (no cracking or bending), but it has negative effect on the interface of melted and unmelted zones, and on the matrix of two melted zones where the level of generated stresses is high.

Effect of EB Treating on Microstructure and Microhardness of Martensitic (AISI 420) Specimens:

The main purpose of the EB treating on the martensitic (AISI 420) stainless steel was to improve the hardness level of the surface layer according to the role of rapid heating by high concentrated energy source and the self-

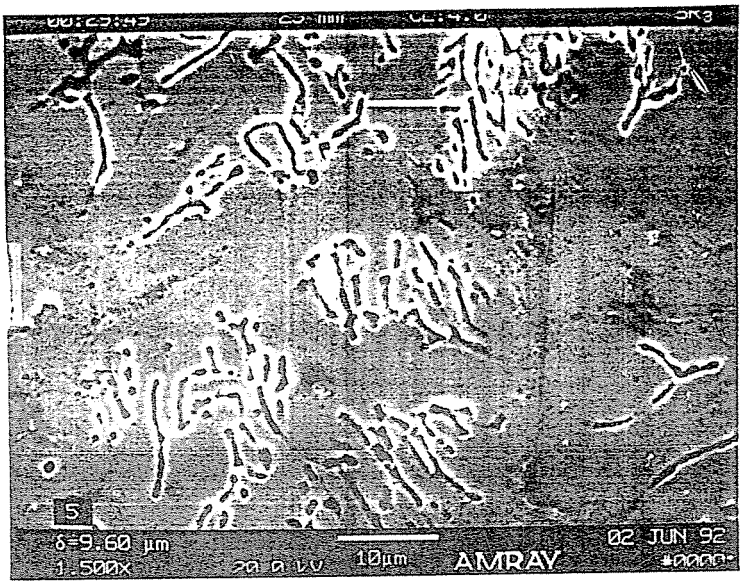

Technology (5E)

Technology (7E)

Fig. 9. Measurement of dendrite arm spacing of EB melted layers, at the same depth position from the surface of (0.5 mm)

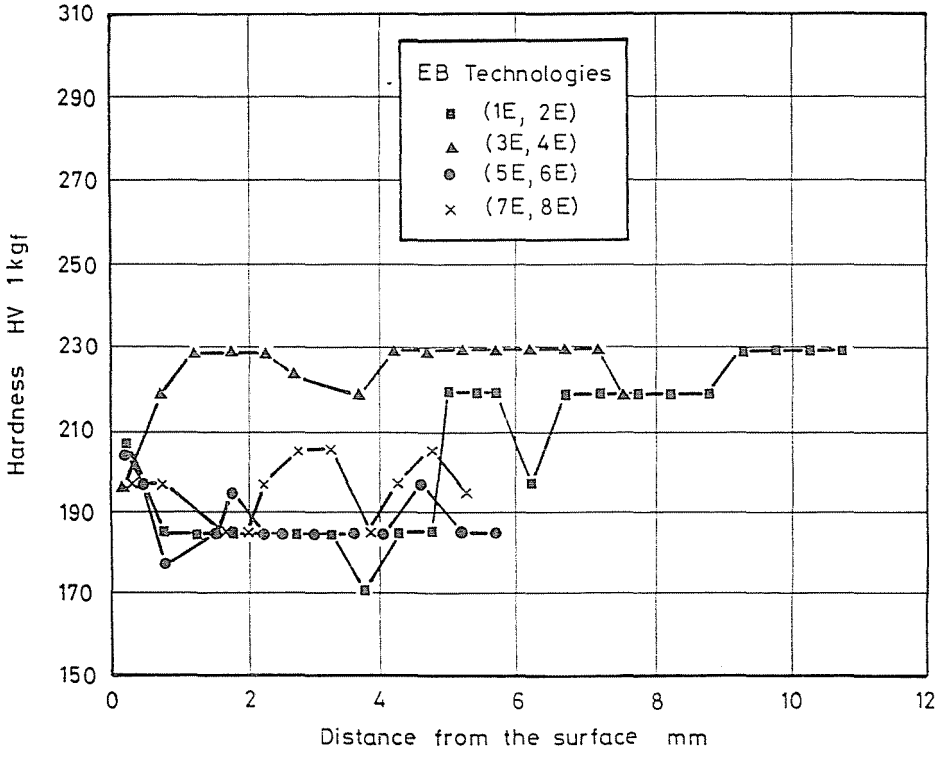

Fig. 10. Hardness profiles of austenitic (AISI 321 Ti) specimens, after EB melting.

quenching of the selected specimens, however, their dimensions and the thin treated surface layers by suitable EB parameters increase the hardness of this hardenable material. The rapid cooling after this high concentrated energy heat processing created a new microstructure in a very thin surface layer (see *Table 3*), using the random multi-points EB deflection *(Fig. 3)*, since the distribution of uniformly tracks were occurred during short period time.

As a result of creation of this new microstructure in the surface layers of our martensitic specimens, the hardness levels were modified to become

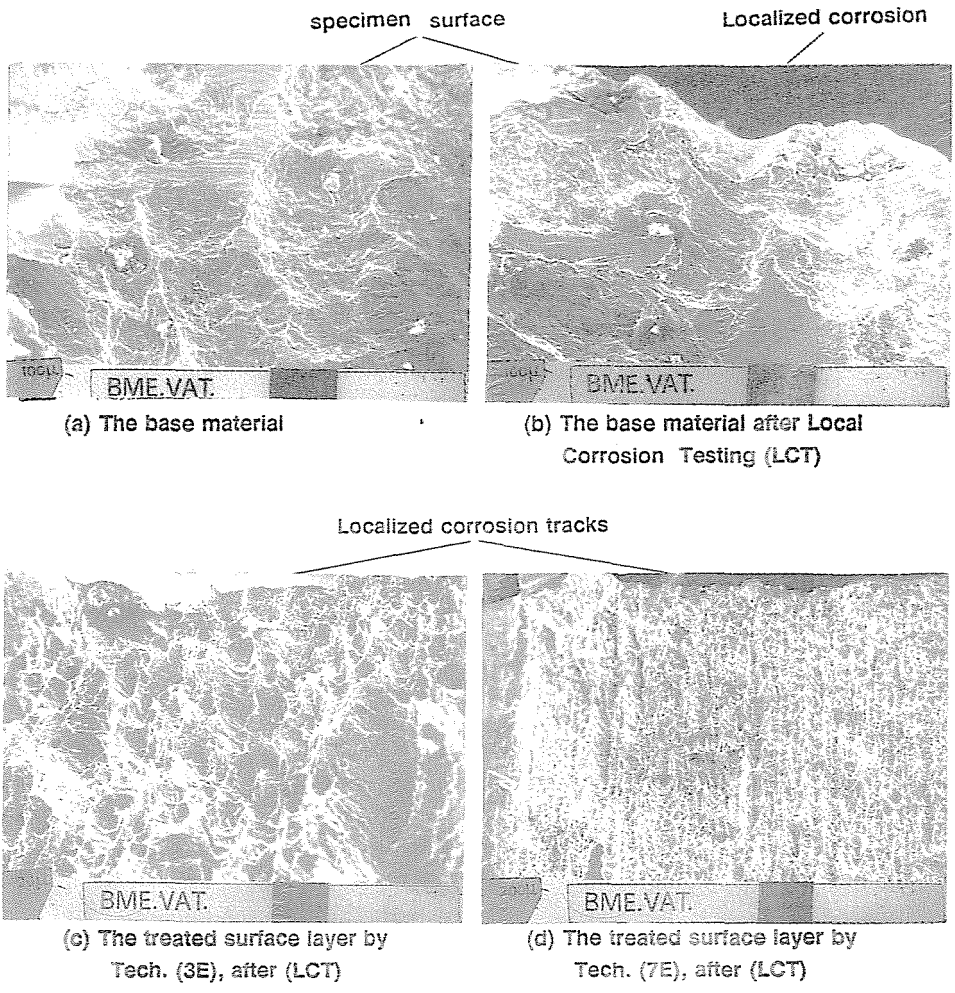

Fig. 11
(SEM) Micrographs of Charpy non-standard fracture surfaces of austenitic (AISI) specimens.

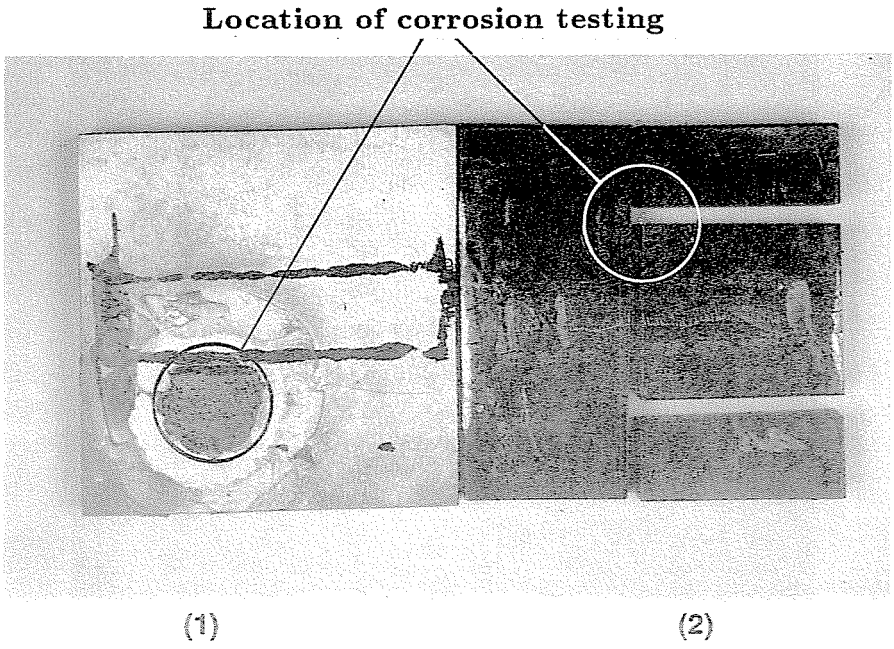

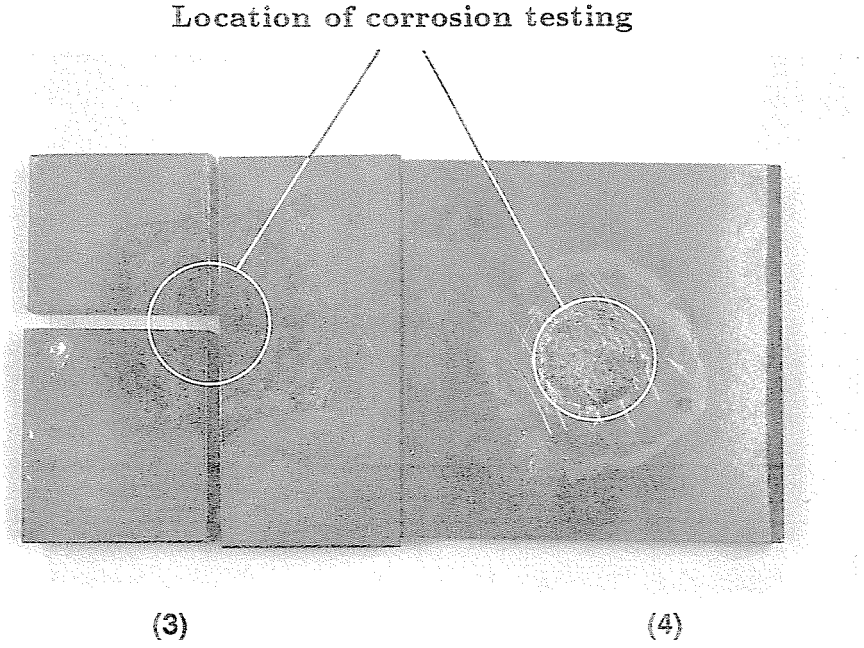

Fig. 12 Localized corroded surfaces of austenitic (AISI 321 Ti) specimens of
1) EB melted layer by Tech. (3E, 4E)
2) EB melted layer by Tech. (3E, 4E)
3) EB melted layer by Tech. (1E, 2E)
4) EB melted layer by Tech. (7E, 8E)

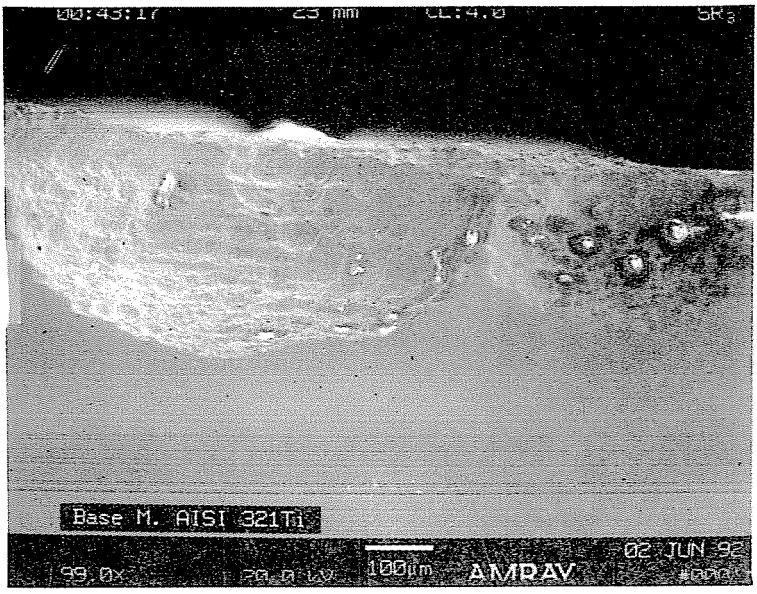

(a)

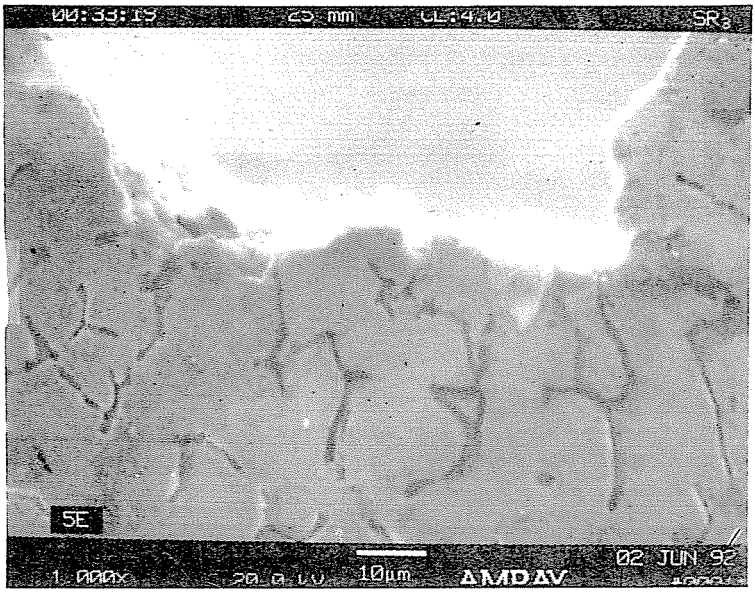

(b)

Fig. 13 (SEM) Micrographs of the corroded surface layers of austenitic (AISI) specimens of:
a) The base material
b) EB melted by Tech. (5E)

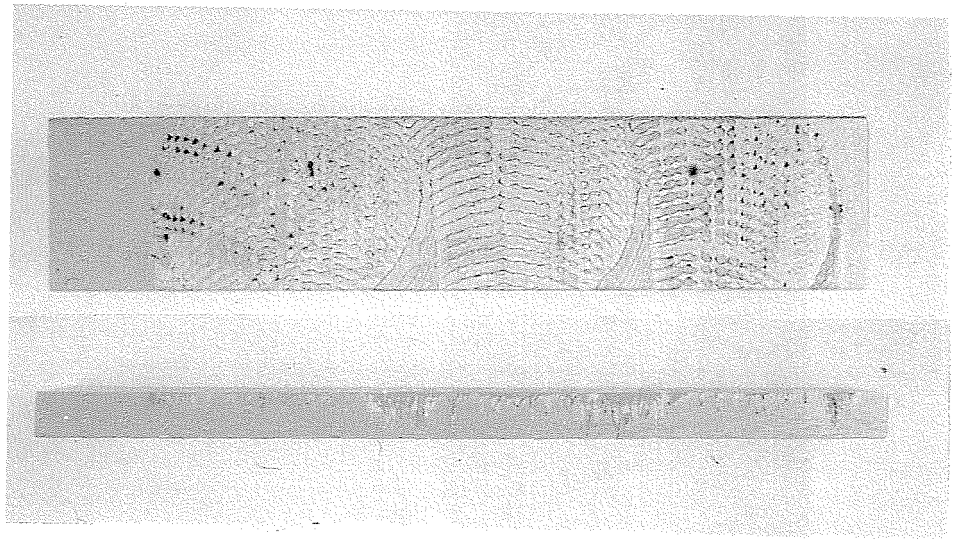

(a)

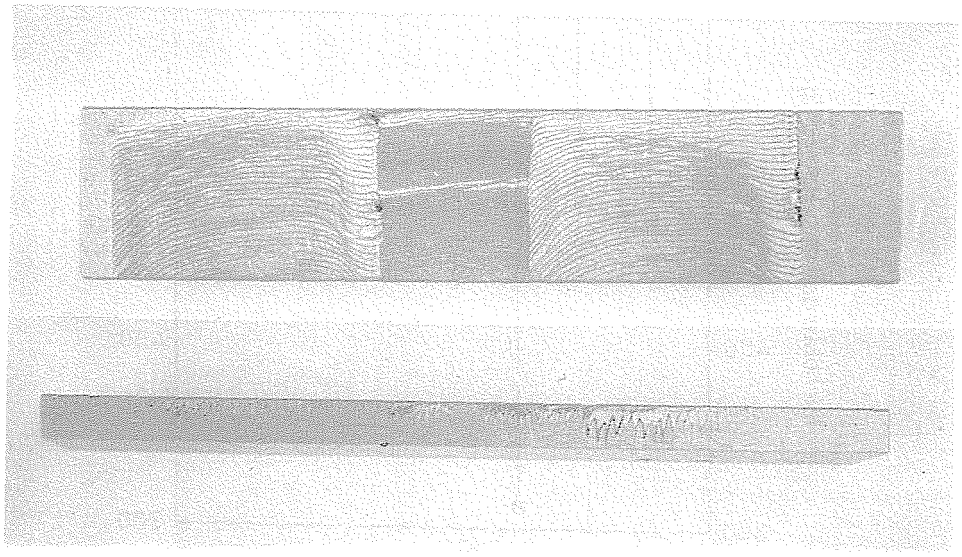

(b)

Fig. 14 Intergranular corrosion testing of austenitic (AISI 321Ti) specimen of:
a) EB melting by Tech. (3E)
b) EB melting by Tech. (1E)

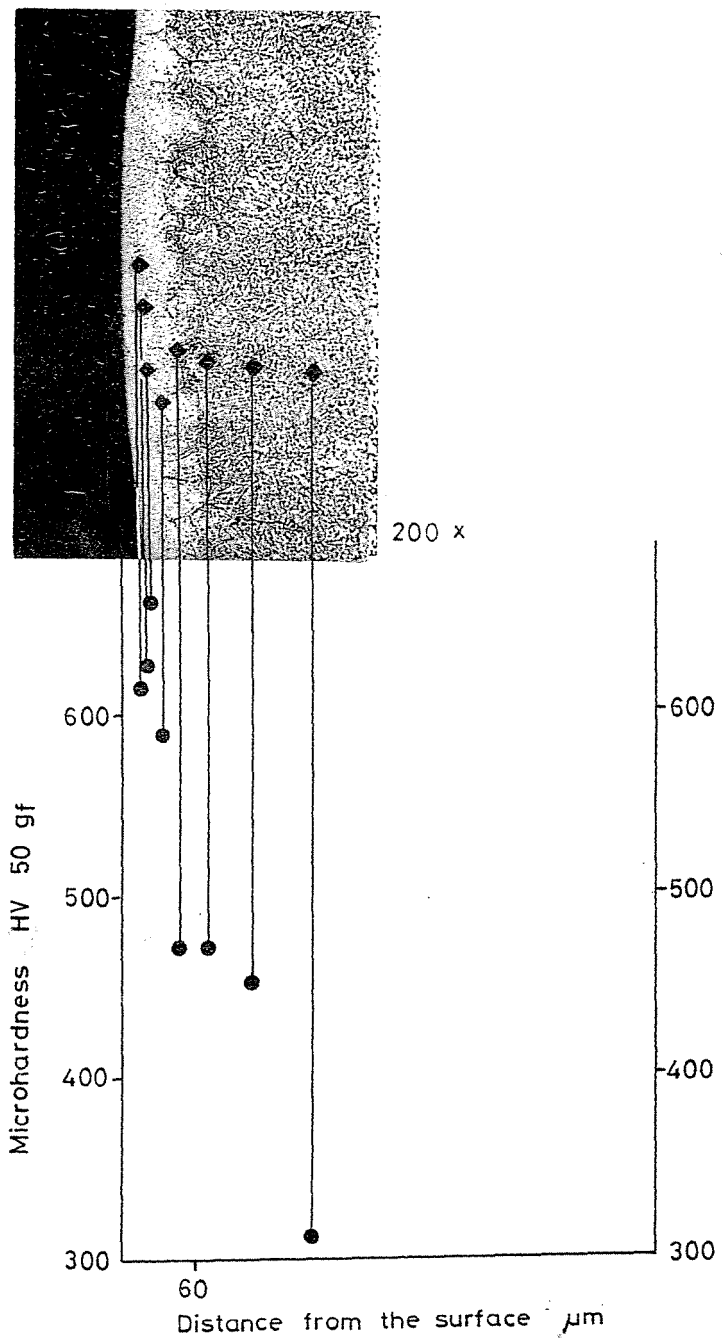

Fig. 15 (OM) Micrograph, microhardness profile of martensitic (AISI 420) specimen, after EB Tech. (1E) surface treating.

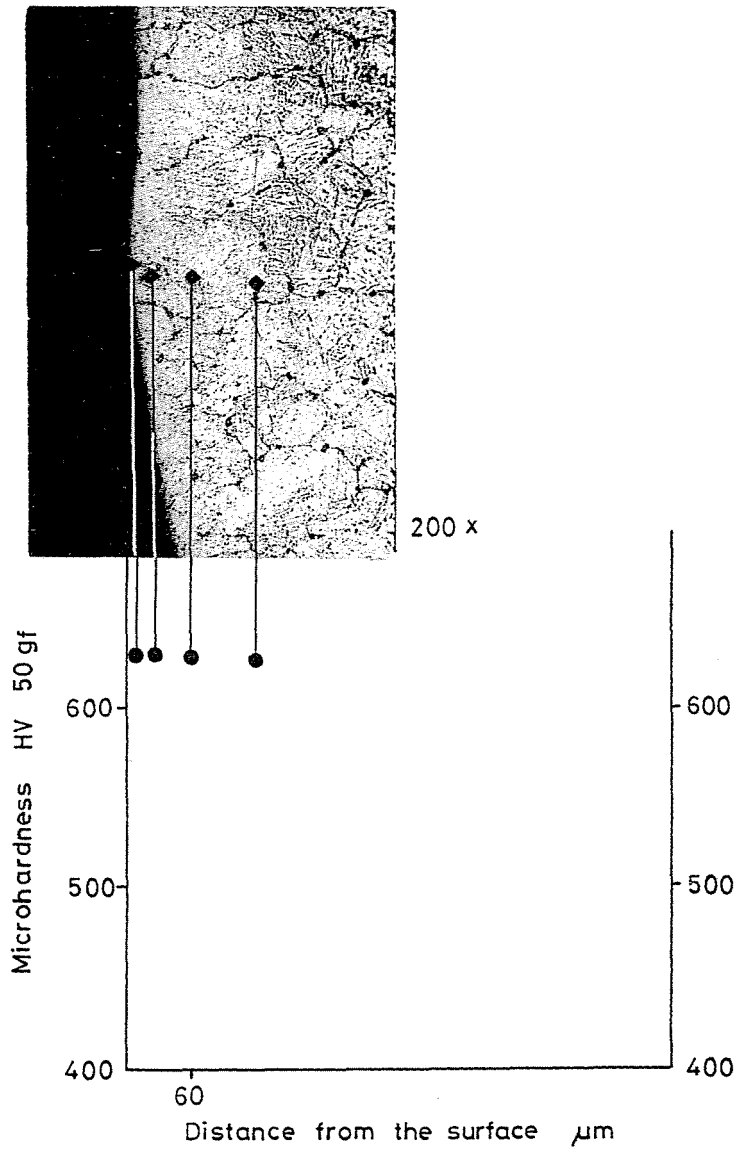

Fig. 16 (OM) Micrograph, microhardness profile of martensitic (AISI 420) (AISI 420) specimen, after EB Tech. (2E) surface treating.

Table 3
Parameters and shapes of EB surface treatments for martensitic specimens

No. of tech.	I_f [A]	I_b [mA]	U [mm/min]	V f/s	EB deflection	Depth of melted layer [μm]
1E	0.806	108	60	1 period, $t = 120$ s	multi-points	60
2E	0.806	108	60	1 period, $t = 40$ s		—

in the range of (317 to ~600 HV), while the hardness of the base material is (~250 HV).

Figure 15 and *Fig. 16* show the microstructure of surface layers treated by technologies (1E & 2E), respectively, with indentations of microhardness measurement of [HV 50 gf], as well as the microhardness distribution across section of these layers. However, the cooling rate in the first case is lower than that in the second one, because of the difference in the heating period time, (120 s for technology 1E, and 40 s for 2E), (*Table 3*). Thus, the depth of treated and transformation zones are different, too.

Conclusions

– The EB surface treating offers good possibility to modify the microstructure of the surface layer of (AISI 321Ti) to fine dendritic microstructure as a consequence of the rapid solidification. The refinement of microstructure (dendrite arm spacing) depends on depth of the treated surface layer which is related to the EB parameters, consequently, the corrosion resistance of refined surface layer is better than that of the base material.

– Corresponding to changes in modes of solidification and morphologies of microstructure, the hardness of the treated layers of (AISI 321Ti) is higher than its base material in different range of (30–40 HV), with high improvement of the toughness in melted layer as opposed to the base material.

– The EB treated surface layers of (AISI 420) have higher hardness in range (350–400 HV), than the base material has. The suitable shape pattern of EB deflections is random multi-points shaped because of its high cooling rate as well as the smooth tracks of EB melting.

– During the higher cooling rate solidification, which greatly depends on the chemical composition, it can be seen that the cooling rate tends to become higher when Cr_{eq}/Ni_{eq} content of alloys is higher, thus, the cooling rate of (AISI 420) must be higher than that of (AISI 321Ti). The more

refinement microstructure of (AISI 420) is a good evidence for the difference in the cooling rates at solidification.

Acknowledgement

This work was supported by the Hungarian Academy of Science and sponsored by the Department of Mechanical Engineering and Material Science of the Technical University of Budapest The author gratefully acknowledges the financial and technical support provided by them. Furthermore, the author would like to thank the Institute of Industrial Technology (ITI) and Metal Control-Ld of Miskolc that significantly contributed to the treating and microstructural studies.

References

1. ARTINGER, I.: Phase Transformation and Changes of Properties in Case of Treatments with High Power Density, *Gépgyártástechnológia,* XXVIII. Vol. 7. 1989. Júli, pp. 327–332, (in Hungarian).
2. ARATA, Y.: Plasma, Electron & Laser beam Technology, *Development and Use in Material Processing,* (AMS, Copyright), 1986.
3. ARTINGER, I. – KORACH, M. – PAHOMOVA, N. A.: Changes in Materials Structure during Surface Treatment by High Energy Sources, Proc. of 5^{th} Int. Conf. (Heat Treatment of Materials), Budapest, October, 1986, pp. 1533–1542.
4. HICK, A. J.: *Heat Treatment of Metals,* Vol. 1, 1983, p. 3.
5. MAZUMDER, J.: *Journal of Metals,* Vol. 5, 1983, p. 8.
6. SHIUE, R. K. – CHEN, C.: *Scripta Met.,* Vol. 25, 1991, pp. 1890–1894.
7. YANG, L. J. – JANA, S. – TAM, S. C.: *Journal Material Proc. Tech.* Vol. 21, 1990, pp. 119–130.
8. NAKAO, Y. – NISHIMOTO, K. – ZHANG, WEN-PING: *Trans. J. W. S.,* Vol. 19. No. 2, Oct. 1988, pp. 20–26.
9. ANTHONY, T. R. – CLINE, H. E.: *J. Appl. Phys.* Vol. 49, 1978, p. 1248.
10. LUMSDEN, J. B. – GNANAMUTH, D. S. – MOORES. R. J.: Fundamental Aspects of Corrosion Protection by Surface Modification, E. McCafferty, C. R. Clayton and J. Ouder eds., The Electrochemical Society, Pennington, NJ, 1984, p. 122.
11. Metals Handbook, (ASM), Ninth Edition, Vol. 13, 'Corrosion', 1987, p. 231.
12. HATFIELD, W. H.: *J. Iron Steel Inst.,* Vol. 127., 1933, pp. 380–383.
13. HUEY, W. R.: *Trans. Am. Soc. Steel Treat.,* Vol. 18, 1930, pp. 1126–1143.